ANNALI DI GEOFISICA, VOL. XXXVII, N. 6, December 1994

A comparison of two methods for earthquake source inversion using strong motion seismograms

Brian P. Cohee and Gregory C. Beroza
Department of Geophysics, Stanford University, Stanford, CA, U.S.A.

Abstract
In this paper we compare two time-domain inversion methods that have been widely applied to the problem of modeling earthquake rupture using strong-motion seismograms. In the multi-window method, each point on the fault is allowed to rupture multiple times. This allows flexibility in the rupture time and hence the rupture velocity. Variations in the slip-velocity function are accommodated by variations in the slip amplitude in each time-window. The single-window method assumes that each point on the fault ruptures only once, when the rupture front passes. Variations in slip amplitude are allowed and variations in rupture velocity are accommodated by allowing the rupture time to vary. Because the multi-window method allows greater flexibility, it has the potential to describe a wider range of faulting behavior; however, with this increased flexibility comes an increase in the degrees of freedom and the solutions are comparatively less stable. We demonstrate this effect using synthetic data for a test model of the M_w 7.3 1992 Landers, California earthquake, and then apply both inversion methods to the actual recordings. The two approaches yield similar fits to the strong-motion data with different seismic moments indicating that the moment is not well constrained by strong-motion data alone. The slip amplitude distribution is similar using either approach, but important differences exist in the rupture propagation models. The single-window method does a better job of recovering the true seismic moment and the average rupture velocity. The multi-window method is preferable when rise time is strongly variable, but tends to overestimate the seismic moment. Both methods work well when the rise time is constant or short compared to the periods modeled. Neither approach can recover the temporal details of rupture propagation unless the distribution of slip amplitude is constrained by independent data.

Key words *earthquake source inversion – rupture propagation – strong ground motion*

1. Introduction

Inverse methods have been applied to estimate the rupture time and slip amplitude using near-source (< 200 km) strong motion seismograms for many well-recorded earthquakes (*e.g.* Olson and Apsel, 1982; Hartzell and Heaton, 1983; Fukuyama and Irikura, 1986; Takeo, 1987; Beroza and Spudich, 1988; Hartzell, 1989; Mendez and Luco, 1990; Mendez and Anderson, 1991; Cocco and Pacor, 1993). The common goal in this research is to estimate the spatial and temporal distribution of coseismic slip on an assumed planar fault surface or surfaces by matching recorded seismograms with theoretical seismograms. The kinematic rupture models derived in this way provide important constraints on the dynamics of earthquake rupture (*e.g.* Heaton, 1990; Scholz, 1990). Moreover, an accurate description of earthquake rupture aids in understanding the strong ground motion, leading to an enhanced ability to design structures that withstand strong motion in future earthquakes.

Despite much research in this area, there remain important discrepancies between rupture

models of the same earthquake published by different authors. It is typically difficult to assess the relative accuracy of each model. For the most part, past studies have concentrated on deriving a model that fits the strong motion data, without much emphasis on assessing the solution stability or spatial resolution. Using standard inverse methods, it is not difficult to obtain a solution that matches the data acceptably well. The greater challenge lies in estimating the reliability. Some solution discrepancies are due to differences in the portion or bandwidth of the wavefield used in the inversion. However, an under-appreciated source of model discrepancies result from the different model parameterizations and inversion methods. It is important to understand the origin of the model differences because they often have more to do with assumptions made in the modeling than with the earthquake.

Examples of recent earthquakes where authors using similar strong-motion data have found dissimilar solutions include: the 1979 Imperial Valley earthquake (Olson and Apsel, 1982; Hartzell and Heaton, 1983), the 1984 Morgan Hill earthquake (Hartzell and Heaton, 1986; Beroza and Spudich, 1988), the 1987 Superstition Hills earthquake (Frankel and Wennerberg, 1989; Wald *et al.*, 1990), the 1989 Loma Prieta earthquake (Beroza, 1991; Steidl *et al.*, 1991; and Wald *et al.*, 1991), and the 1992 Landers earthquake (Cohee and Beroza, 1994; Wald and Heaton, 1994). In fact, all earthquakes that have received more than one published study show some significant differences in the derived models. These discrepancies are often cited as indicative of the amount of uncertainty in rupture models obtained from strong-motion data.

Frankel (1992) suggested in the case of the 1987 Superstition Hills earthquake that differences in the data and data weighting were the cause of solution discrepancies, noting in particular that without applying some weighting, close stations with larger seismogram amplitudes dominated the least-squares inversion. In this example, the model parameterizations and inverse methods were very different (Frankel and Wennerberg, 1989, solved for a line-source using impulsive Green's functions) and it was not easy for identical data and weighting to be used with each inversion method. Dissimilarities in the rupture solutions of the 1989 Loma Prieta earthquake were briefly discussed by Wald *et al.* (1991). They also speculated that differences in the particular stations used and the data weighting, and to a lesser extent the Green's functions, might have been responsible; however they did not assess the relative importance of each or identify features attributable to the different inversion methods.

In this study we compare two established time-domain inversion methods using identical data, weighting, and Green's functions. This allows us to isolate the effect of the model parameterization and inversion method on the solution. We conduct sensitivity tests for each method using synthetic data computed for a hypothetical 1992 Landers, California earthquake with known source properties. The synthetic test model includes variations in slip amplitude, rupture velocity, and rupture duration (displacement rise time), and we determine how well the two different parameterizations recover the known rupture model in the presence of realistic noise.

We find that although the *multi-window method* contains greater flexibility and has the potential to fully describe the wide range of faulting behavior included in the synthetic test case, the results are less stable and much of the noise is incorrectly mapped into source properties. The multi-window method works best when the rise time is strongly variable, but also systematically overestimates the seismic moment. The *single-window method* does a better job of recovering the input moment and the average rupture velocity. Neither method can reliably recover detailed rupture time variations unless the slip model is known independently (*e.g.* from geodetic data).

These two inversion methods were used to model the M_w 7.3 Landers, California earthquake in Cohee and Beroza (1994), yielding slip distribution models that exhibit large-scale similarity. There are similarities in the rupture time models as well, but because of the tradeoff between the slip amplitude and the rupture time, the detailed images of rupture propagation are not reliable using either approach.

2. Rupture model parameterization

The two inverse methods we compare in this paper have been described in previous studies (*e.g.* Hartzell, 1989; Cohee and Beroza, 1994). The most significant difference between the methods is how rupture propagation is represented. In the multi-window approach, each element of the fault is allowed to rupture a fixed number of times. This approach was introduced by Olson and Apsel (1982) and has been used in many later studies.

By allowing each element to rupture more than once, the multi-window model has the flexibility to accommodate variations in both the rupture velocity and the duration of the slip-velocity function (fig. 1). However, with this flexibility, the number of unknowns increases with the number of time windows used. If the uncertainty in the data and modeling were known, the significance of the additional degrees of freedom could be assessed statistically.

In the single-window parameterization, each fault element ruptures only once but rupture time variations are allowed by admitting perturbations to a constant-rupture-velocity starting model (Fukuyama and Irikura, 1986; Takeo, 1987; Beroza and Spudich, 1988; Hartzell and Iida, 1990). The perturbations are found in a separate, nonlinear inversion. In this approach, the rise time is assumed to be constant over the entire fault and is optimized by finding the value which produces the best overall fit to the data.

Both methods improve the fit to data by allowing some rupture time variation. This is accomplished by an increase in the model dimension, which results in a decrease in the solution uniqueness. An advantage of the single-window method is that it can accommodate larger variations in rupture time with fewer model parameters than the multi-window method because there are only two model parameters per grid point (displacement amplitude and rupture time). An advantage of the multi-window method is that it allows the source time function (and rise time) to vary across the fault surface.

3. Inversion

The inversion method used to estimate a model from data is necessarily different for the single- and multi-window methods because the relationship between the data and the model parameters is different. The seismograms are linearly related to the slip amplitude for both models, but are nonlinearly related to the rupture time (Spudich, 1980). Thus we can solve for the slip amplitude using a linear inversion in both cases; however, to solve the nonlinear problem for rupture time, we choose to linearize the problem.

In the present application of the multi-window method, slip occurs at each element in three adjacent time-windows each separated by 2 s. In the single-window method each element slips once, when the rupture front passes. The rise time is a constant 2 s (note that the data is filtered removing signal at periods shorter than 4 s). Two desirable attributes of the multi-window model are that modest deviations from the assumed rupture velocity are accommodated, and the rise time at each element can vary within a prescribed range (in this case 2 to 6 s).

For the linear inversion we assemble a system of equations of the form $\boldsymbol{Am} = \boldsymbol{d}$. The kernel A is a $N \times M$ matrix relating slip amplitude at each point on the fault to recorded seismograms, $\boldsymbol{m}$ is the model vector of slip amplitude with length M, and $\boldsymbol{d}$ is the data vector of length N. Displacement seismograms for the three components of motion form $\boldsymbol{d}$. For each seismic station, theoretical seismograms representing the contribution from each fault element comprise the columns of the $\boldsymbol{A}$ matrix. The size of N is the product of the number of stations, number of components, and the number of points in each seismogram. When we restrict each element to slip once, the size of the model space M is simply the number of fault elements. When slip is permitted to occur on the same element in adjacent time windows, the size of the model space is multiplied by the number of windows. In the linearized inversion for rupture time, each element slips once and we solve for the optimal rupture time of each element assuming a fixed slip distribution.

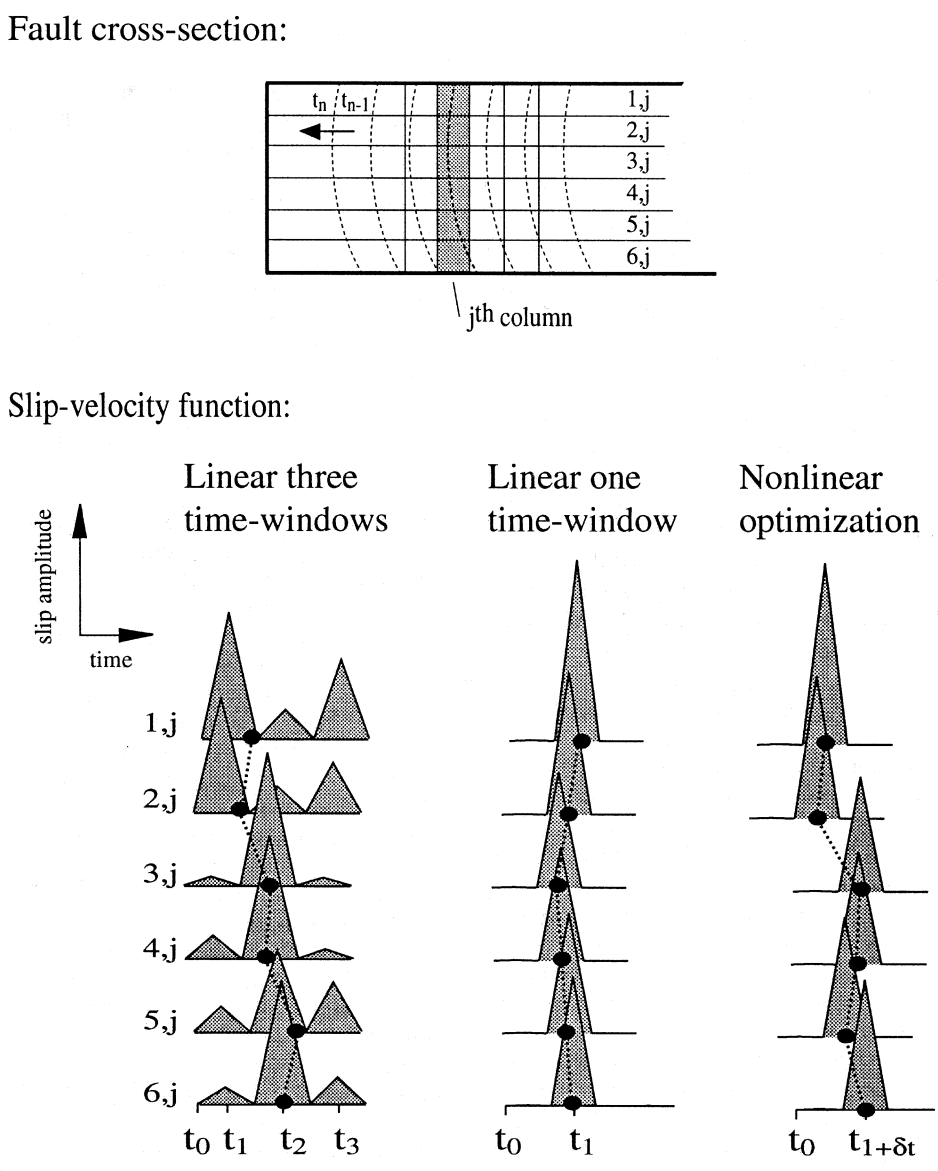

Fig. 1. Schematic cartoon showing the single and three time-window rupture parameterizations. A cross-section of a rectangular fault plane is shown at the figure top and is divided into square fault elements. The rupture propagates from right to left. Below the cross-section, example slip-velocity functions are shown for the j^{th} column of fault elements. The slip-velocity functions used in this study are triangular and symmetric. The width of the triangle is the displacement rise time. The linear three time-window method has the flexibility to unevenly distribute the slip across the three windows. With this method, it is helpful to define the slip-weighted temporal centroid for each element. The centroid is shown schematically. In the single time-window method each element slips once, and the timing of the slip is optimized with a nonlinear inversion. In this cartoon both the multi-window and the nonlinear model show early rupture of the 2, j element, but differ in the rupture time of the 5, j element.

Consequently, the solution to the linearized problem requires an additional M model parameters. The number of model parameters in the multi-window inversion is M times the number of time windows. In the present example it is 3 M.

We solve the linear problem for slip amplitude using both model parameterizations. The three-window method solves for both the slip distribution and rupture time in one step. The possible rupture time at each element is limited to the specific time-windows used, so the rupture velocity of the first window is an upper bound on the average rupture velocity. Likewise, variation in the time function is limited to the assumed window spacing (see fig. 1). In contrast, the linear single time-window result is obtained using a constant rupture velocity, so we perform a separate, linearized inversion to optimize the rupture time of each fault element. This second method is similar to the *linearized inversion* of Beroza and Spudich (1988) and the *nonlinear inversion* of Hartzell (1989), except they solved for both the slip amplitude and rupture time simultaneously. The difficulty with this simultaneous approach is that it is unclear how to weight the two groups of unknowns. Because of the strong trade-off between the slip amplitude and rupture time, it is difficult to solve this relative weighting problem without independent information on either component of the solution. One approach toward resolving this ambiguity is to use geodetic data to estimate the static slip distribution, and seismic data to estimate the temporal characteristics of rupture (Cohee *et al.*, 1993).

We do not have quantitative information on the uncertainties in the data, so it is not obvious what weighting is most appropriate for the inversion. In the absence of data covariance, the weighting is necessarily somewhat arbitrary. In this study, we normalize the three components of motion at each station by the total power at that station. With this scheme, each station has equal weight and the contribution of the vertical component is the smallest. The weighting matrix is defined $\boldsymbol{R} \equiv \text{diag}\,[1/\text{power}^{\text{sta}}]$, where $\text{power}^{\text{sta}}$ is the summed power of the three components at each station.

The size of the model space in each of the parameterizations is large and it is therefore important to enhance the solution stability by regularizing the linear system. An example of this stability problem is found in Hartzell (1989). He used the multi-window approach and found that the earthquake moment increased with the addition of each time window. One technique to overcome this particular problem is to append a moment minimization constraint (Hartzell and Heaton, 1983). A more widely used regularization method is to require that the solution be spatially smooth. In earthquake source inversions, this is accomplished by simultaneously minimizing either the first or second spatial derivative of the model (or perturbations to the model).

We apply three types of regularization to the problem. We append a smoothing constraint that minimizes the slip amplitude gradient (first derivative) of $\boldsymbol{m}$. This augmented linear system is written

$$\begin{pmatrix} \boldsymbol{RA} \\ \varepsilon_0 \boldsymbol{D} \end{pmatrix} \boldsymbol{m} = \begin{pmatrix} \boldsymbol{Rd} \\ 0 \end{pmatrix},$$

where $\boldsymbol{D}$ is the smoothing matrix and ε_0 is a scalar that weights $\boldsymbol{D}$. There is a predictable trade-off between model roughness, defined as $\|\boldsymbol{Dm}\|^2$, and data fit – a rougher model fits the data better, but is less stable. With the Landers earthquake, we have the benefit of independent observations of surface displacement that is used to estimate the best smoothing weight (Cohee and Beroza, 1994). Furthermore, we can constrain the top of the model to match the amplitude of slip, $\boldsymbol{s}$, mapped at the surface, however we do not use this constraint in the synthetic test cases. Additionally, we prescribe a homogeneous boundary condition at the bottom of the fault plane. This new system is written

$$\begin{pmatrix} \boldsymbol{RA} \\ \varepsilon_0 \boldsymbol{D} \\ \tau \boldsymbol{T} \\ \gamma \boldsymbol{B} \end{pmatrix} \boldsymbol{m} = \begin{pmatrix} \boldsymbol{Rd} \\ 0 \\ \tau \boldsymbol{s} \\ 0 \end{pmatrix}.$$

When the boundary conditions are enforced $\gamma = \varepsilon_0/2$, and τ is chosen so the model slip am-

plitudes at the ground surface match the observations within a prescribed tolerance. For both the multi-window and the linear first-step of the single-window inversion, the system is solved using the non-negative least squares algorithm of Lawson and Hanson (1974).

To optimize the rupture time in the single-window method, we adopt a Newton-Raphson linearization (Press *et al.*, 1989) and iteratively solve for perturbations to a starting model of rupture time. The strength of this approach is that we improve the fit to data with relatively small changes (< 2 s) in the rupture time of each element, the weakness is that we only find the minimum closest to the starting model, which may not be the global minimum. We solve for perturbations $\boldsymbol{dm}$ to the starting rupture time model $\boldsymbol{m}$. The linearized system is written $\boldsymbol{g}(\boldsymbol{m}+\boldsymbol{dm}) = \boldsymbol{g}(\boldsymbol{m}) + \boldsymbol{Jdm}$, where $\boldsymbol{J}$ is the Jacobian matrix of partial derivatives relating change in the rupture time model to each of the residual seismograms:

$$J_{ij} = \frac{\partial g_i}{\partial m_j},$$

and $\boldsymbol{g}(\boldsymbol{m})$ is the functional that yields synthetic seismograms for a given rupture and slip model. The Jacobian matrix is computed using a fourth-order central difference operator with error proportional to $(\Delta t)^4$, where Δt is the sampling interval of the data. The linearized system is written as

$$\begin{pmatrix} \boldsymbol{RJ} \\ \varepsilon_1 \boldsymbol{D} \end{pmatrix} \delta \boldsymbol{m} = \begin{pmatrix} \boldsymbol{Rr} \\ 0 \end{pmatrix},$$

where the residual $\boldsymbol{r} = \boldsymbol{d} - \boldsymbol{g}(\boldsymbol{m})$, and again we impose the first-derivative smoothing operator $\boldsymbol{D}$ (weighted by ε_1) that in this case smoothes the rupture time perturbation field. We iterate on $\boldsymbol{m}_n = \boldsymbol{m}_{n-1} + \boldsymbol{dm}_n$ until a convergence criterion is met. At each iteration the system is solved using either a SVD (Press *et al.*, 1989) or a SIRT algorithm (Olson, 1987). We use the efficient SIRT algorithm to evaluate the large range of starting models and smoothing weights.

4. A synthetic test case using the Landers earthquake geometry

4.1. *The Landers earthquake*

We have based our synthetic test case on the strong-motion data set and fault geometry of the M_w 7.3 1992 Landers, California earthquake. The Landers mainshock was the largest earthquake to occur in Southern California since the M_w 7.7 1952 Kern County event. It produced right-lateral displacements at the ground surface for over 70 km on a sequence of right-stepping vertical faults that form the northward extension of faulting that began approximately two months earlier with the M_w 6.1 Joshua Tree earthquake (Hauksson *et al.*, 1993).

The location of the fault used in our model is based on the surface trace of mapped rupture (Ponti, 1992; Sieh *et al.*, 1993; Johnson *et al.*, 1994) and aftershock locations (Hauksson *et al.*, 1993). The rupture surface is represented with three planar segments that extend vertically from the surface to a depth of 18 km. The location of the assumed fault segments are shown in fig. 2. The hypocenter is assumed to be at 34.20°N latitude and 116.43°W longitude at 4.5 km depth (Hauksson *et al.*, 1993). In this parameterization, the southern segment of the fault is 27 km in length and strikes 354°, the middle segment is 30 km long and strikes 331°, and the northern segment is 45 km long with a strike of 322°. These three segments represent the Johnson Valley, Homestead Valley, and Camp Rock-Emerson faults, respectively (Johnson *et al.*, 1994). The representation of the rupture surface as three planar segments is an idealization, however because only longer period energy (≥ 4 s) is used in this analysis, error introduced by this simplified fault parameterization is small. It is important to recognize that in the sensitivity tests the synthetic data is calculated using the same geometry, slip-velocity function, and Green's

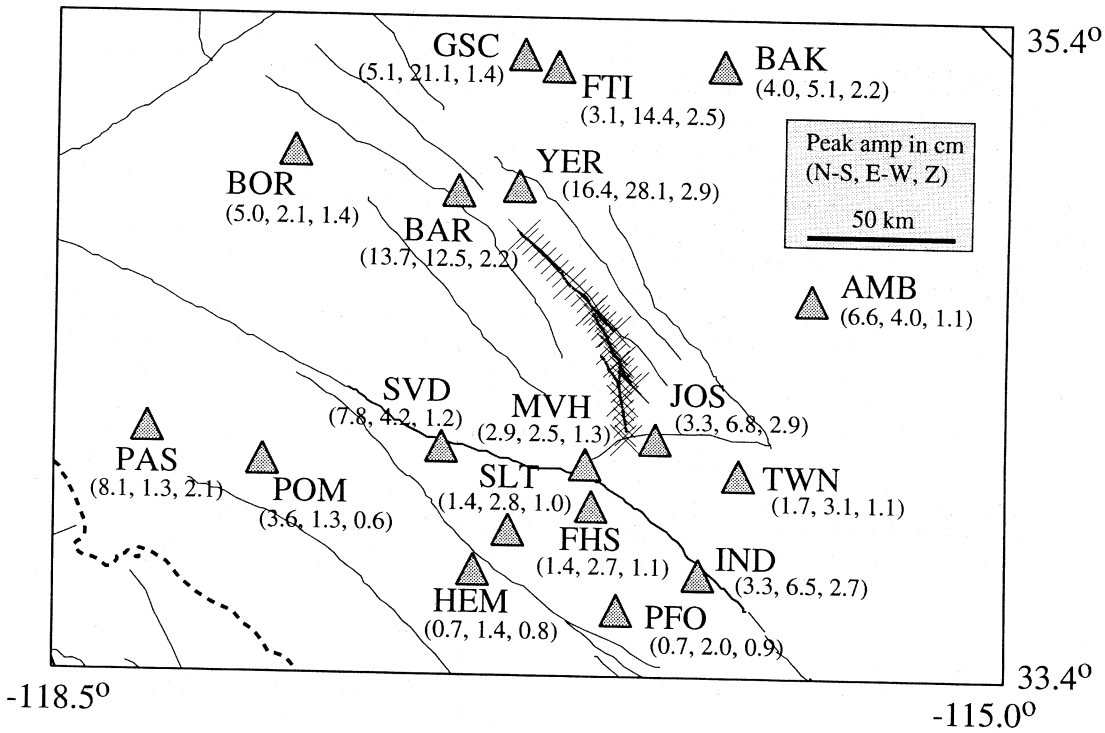

Fig. 2. Map of the 18 low-gain, accelerometer stations used in this study. The stations are identified by three-letter code and are listed in table I. Peak displacements (cm) for each component at each station are listed below the station code. The mainshock rupture zone is indicated by symbols that show the surface projection of each fault element. The symbols form three linear fault segments, representing (from south to north) the Johnson Valley, Homestead Valley, and Camp Rock-Emerson faults.

functions used in the inversion, consequently there is no modeling error.

The Landers earthquake was recorded by the TERRAscope array and triggered numerous low-gain accelerometers in the near-source region. Source mechanisms determined from regional first motion data and teleseismic surface waves indicate almost pure right-lateral strike-slip displacement on a vertical fault (Hauksson *et al.*, 1993). There are large right-lateral offsets ($\leq$ 6 m) and discontinuous vertical displacement (< 2 m) mapped at the surface, however the vertical slip is believed to be mostly influenced by the topography and near-surface geology (Sieh *et al.*, 1993; Johnson *et al.*, 1994).

In our Landers earthquake model, we subdivide the three fault segments into 204 (3×3 km^2) elements. Where the fault segments overlap, the slip occurs simultaneously on both segments.

We use this parameterization to find the best average rupture velocity from a range of plausible values (1.8 to 3.5 km/s). The rupture is assumed to initiate at 4.5 km depth at the location determined from the high-frequency network (Hauksson *et al.*, 1993), and we adopt a 3 s delay to the published origin time (11:57:34.1 UTC) to account for the delay between this origin time and the initiation of mainshock rupture as discussed in Abercrombie and Mori (1994) and Dreger (1994).

4.2. *Strong-motion data*

The 18 near-source, low-gain stations used in this study come from three sources: TERRAscope (Kanamori *et al.*, 1992), the California Strong Motion Instrumentation Program (CSMIP, 1992), and the United States Geological Survey (Hough *et al.*, 1993). The station name, location, and other characteristics are listed in table I, and their areal distribution is shown in fig. 2. The different recording characteristics of these seismic stations influence several aspects of the modeling effort.

The four TERRAscope sites (GSC, SVD, PFO, PAS) are equipped with FBA-23 accelerometers. These seismograms are the most useful for three reasons: first and most importantly, recordings from numerous aftershocks are available at the same sites, allowing the accuracy of Green's functions used in the inversion to be evaluated (see Cohee and Beroza, 1994); second, the broadband response of these systems is superior to analog systems, allowing longer periods to be recovered; and third, the data are recorded in absolute time.

The strong-motion seismograms collected by CSMIP were recorded on SMA-1 accelerometers. This group comprises the majority of data used in this study (12 stations) and with two exceptions (BOR, YER) was also recorded in absolute time. The displacement seismograms are derived from the recorded accelerograms by CSMIP and have a long-period response reliable to about 15 s (CSMIP, 1992).

We also use two stations (FHS, MVH) deployed by the USGS to record aftershocks of the Joshua Tree earthquake (Hough *et al.*, 1993). This system consists of a Kinemetrics FBA sensor and a digital GEOS recorder.

Table I. Accelerometer stations.

Code	Station name	Latitude	Longitude	Range (km)	Instrument
AMB	Amboy ◊	34.560	115.743	67-98	SMA-1$^{\Omega}$
BAK	Baker ◊	35.272	116.066	88-129	SMA-1$^{\Omega}$
BAR	Barstow ◊	34.887	117.047	28-100	SMA-1$^{\Omega}$
BOR	Boron ◊	35.002	117.650	83-147	SMA-1
FHS	Fire House §	33.925	116.549	27-94	FBA$^{\Omega}$
FTI	Fort Irwin ◊	35.268	116.684	59-127	SMA-1$^{\Omega}$
GSC	Goldstone †	35.303	116.808	62-133	FBA-23$^{\Omega}$
HEM	Hemet ◊	33.729	116.979	69-114	SMA-1$^{\Omega}$
IND	Indio ◊	33.717	116.156	53-128	SMA-1$^{\Omega}$
JOS	Joshua Tree ◊	34.131	116.314	10-81	SMA-1$^{\Omega}$
MVH	Morengo Valley §	34.053	116.572	17-79	FBA$^{\Omega}$
PAS	Pasadena †	34.148	118.172	143-164	FBA-23$^{\Omega}$
PFO	Pinon Flats †	33.609	116.455	59-130	FBA-23$^{\Omega}$
POM	Pomona ◊	34.056	117.748	116-127	SMA-1$^{\Omega}$
SLT	Silent Valley ◊	33.851	116.852	51-99	SMA-1$^{\Omega}$
SVD	Seven Oaks Dam †	34.104	117.098	62-76	FBA-23$^{\Omega}$
TWN	Twentynine Palms ◊	34.021	116.009	41-108	SMA-1$^{\Omega}$
YER	Yermo ◊	34.903	116.823	18-92	SMA-1

$^{\Omega}$ stations with absolute time; ◊ CSMIP; † TERRAscope; § USGS.

MVH is an important record since it is the closest station west of the hypocenter.

The recorded Landers accelerograms are twice integrated to displacement and high-pass filtered using a zero-phase, eight-pole butterworth filter with a 0.08 Hz (12.5 s) corner. We use a 0.05 Hz (20 s) high-pass filter corner with the TERRAscope seismograms. The high-pass filter corners are required by the increased signal-to-noise ratio at lower frequencies. For all stations, we use a low-pass filter corner at 0.25 Hz (4 s). A low-pass filter is used to provide more accurate Green's functions – this particular corner was determined by modeling aftershock seismograms recorded at TERRAscope (Cohee and Beroza, 1994). In the synthetic test case, we filter the artificial data in an identical manner.

4.3. *Model parameterization*

Using the multi-window model, it is simple to add additional time windows. The data vector $\boldsymbol{d}$ remains unchanged. Columns in the $\boldsymbol{A}$ matrix are repeated (with a time shift) for each additional window, and the size of the model vector $\boldsymbol{m}$ is increased accordingly. The window is delayed by a fixed amount (in this study 2 s) from a reference rupture time. The only deterrence to using many time-windows is the practical limitation of increased memory storage and the added solution instability resulting from the larger model dimension. Alternatively, using one time-window assumes each fault element ruptures just once, and it is only possible to find a variable-slip, constant rupture velocity model. We use a rise time duration of 2 s; however, because of the low frequencies used in this study, any rise time of 3 s or less yields similar results. The model is not sensitive to differences in the rise time duration when less than 3 s because the seismograms are filtered using a 4-s corner.

Adding multiple windows permits variable rupture velocity by allowing slip to occur in adjacent time windows. There are no constraints relating the slip at each element in the adjacent windows. If required by the data, the fault element may repeatedly rupture and stop, or have an extended duration. The degree of rise time complexity depends on the duration and number of windows used. Up to six windows have been used with the multi-window approach (Wald and Heaton, 1994). In the following tests we only use three. The instability we find using three windows will likely be more problematic with additional time windows.

4.4. *Inversion results using synthetic data*

We compute synthetic data for a hypothetical rupture using the Landers fault geometry, add uncorrelated white noise of comparable amplitude to that found from modeling aftershocks, and image the slip distribution and rupture time using each inversion method. For a known model $\tilde{\boldsymbol{m}}$, we calculate synthetic data $\tilde{\boldsymbol{d}}$ by computing the forward problem $\boldsymbol{A}\tilde{\boldsymbol{m}} = \tilde{\boldsymbol{d}}$. We then solve the inverse problem

$$\begin{pmatrix} \boldsymbol{RA} \\ \varepsilon_0 \boldsymbol{D} \\ \gamma \boldsymbol{B} \end{pmatrix} \boldsymbol{m} = \begin{pmatrix} \boldsymbol{R}\tilde{\boldsymbol{d}} \\ 0 \\ 0 \end{pmatrix}$$

for $\boldsymbol{m}$. Next, we add a representative noise vector $\boldsymbol{e}$ and solve

$$\begin{pmatrix} \boldsymbol{RA} \\ \varepsilon_0 \boldsymbol{D} \\ \gamma \boldsymbol{B} \end{pmatrix} \boldsymbol{m} = \begin{pmatrix} \boldsymbol{R}\tilde{\boldsymbol{d}} + \boldsymbol{e} \\ 0 \\ 0 \end{pmatrix}$$

for $\boldsymbol{m}$. We perform this test using each inversion method and compare the solution $\boldsymbol{m}$ to the input model $\tilde{\boldsymbol{m}}$ to assess the spatial resolution and accuracy of each inversion method. The slip distribution that we use for the test case is shown in fig. 3 (top left). The synthetic model has right-lateral displacement of either 0, 2, or 4 m, as shown by the 1 m contours. Note that the three rectangular fault segments are projected onto a single fault plane. The rupture velocity varies along the length of the fault: it is 2.2 km/s on the southern (Johnson Valley) seg-

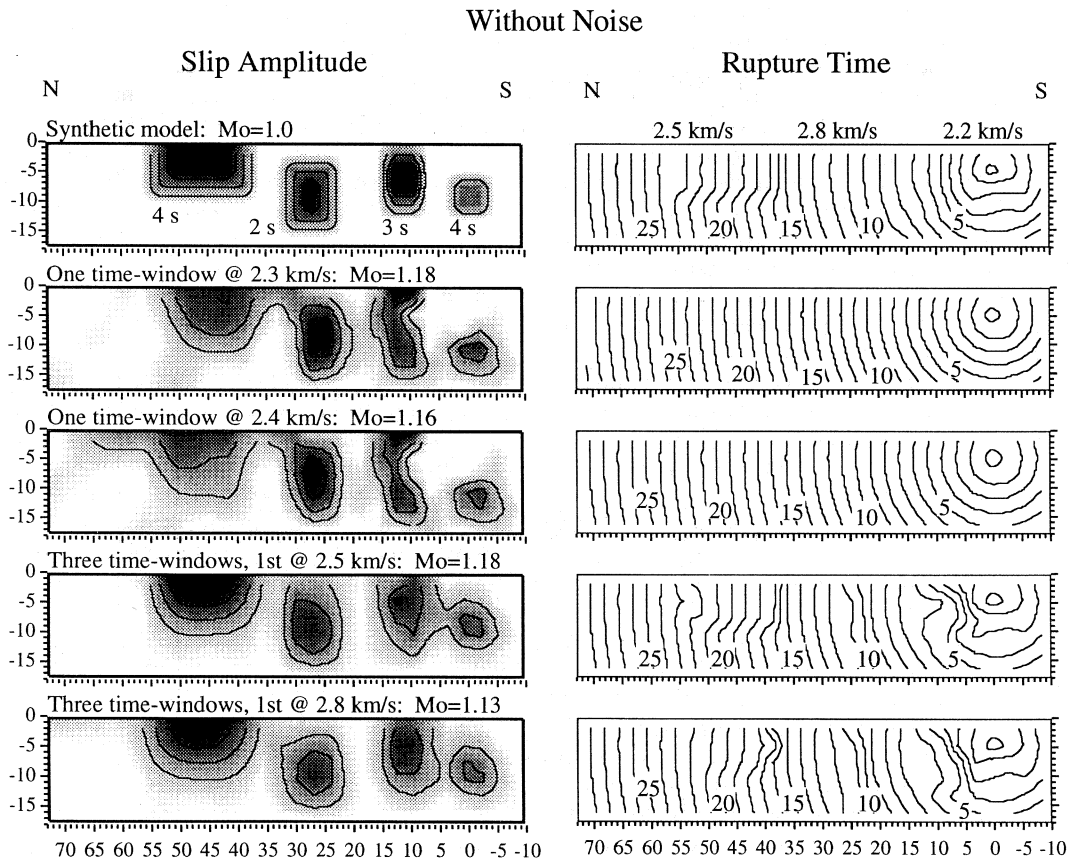

Fig. 3. Input synthetic test model (slip amplitude-top left and rupture time-top right) and the inversion results using the two linear inversion methods. In these cross-section projections of the fault, the overlapping regions are superimposed. The hypocenter is at 4.5 km depth and defines the horizontal origin. The two slip patches in the south fall on the Johnson Valley fault, the center slip patch is on the Homestead Valley fault, and the northernmost patch falls on the Camp Rock-Emerson fault. In each patch, the displacement is right-lateral. The rise time of each patch is either 2, 3 or 4 s, as labeled in the figure (top left). The slip amplitude is either 0, 2, or 4 m (shown by 1 m contours). The second and third panels are the solutions using the one time-window inversion method and a rupture velocity of 2.3 and 2.4 km/s. The fourth and fifth panels are three time-window solutions using rupture velocities of 2.5 and 2.8 km/s, respectively. For these multi-window solutions, the slip-weighted temporal centroid is contoured for those elements with slip above 1 m. For elements with less slip, the rupture time is poorly determined and the 2.5 km/s rupture velocity is contoured. The normalized seismic moment is labeled for each solution.

ment, increases to 2.8 km/s on the middle (Homestead Valley) segment, and decreases to 2.5 km/s on the northern (Camp Rock-Emerson) segment. Additionally, each slip patch has a rise time duration of either 2, 3, or 4 s, which is labeled in fig. 3 (top left). This rupture time model does not contain small-scale perturbations that may occur in earthquake rupture – in this test we only seek to reproduce the average rupture of each segment and the rise time variability. The rupture time for the input model is contoured in fig. 3 (top right).

This strategy of using sensitivity tests for resolution analysis is discussed in Beroza and Spudich (1988) for the earthquake rupture problem, and in Spakman and Nolet (1988) for the delay-time tomography problem. The ability of each inversion method to recover the known slip and rupture model is indicative of the resolution expected with the real data. Artifacts of each method evident with synthetic data are also likely to exist with the recorded data. The range of rupture velocity, rise time, and slip amplitude in the synthetic model is intended to be representative of the variation found in the actual Landers earthquake. The rupture velocity varies from 2.2 to 2.8 km/s; rise times are 2 to 4 s, which is reasonable given the width of the rupture surface (Day, 1982); and the slip is spatially heterogeneous, with large patches of displacement (asperities) separated by areas of zero slip.

The inversion results using the synthetic data without noise are shown in fig. 3. The second and third panels show the slip amplitude distribution obtained using the single-window method and constant rupture velocities of 2.3 and 2.4 km/s, respectively. The fit to the data is nearly identical using either rupture velocity, but the slip distribution is different. The single-window model does a good job of recovering the input slip when the rise time is short (2 to 3 s). When the rise time is longer (0 and 45 km along strike), more of the slip is mislocated in neighboring elements. This is a result of the inability of the single-window method to reproduce the longer rise times. Instead, the method prefers a slower rupture velocity and tends to put greater weight on shallow elements that have lower frequency Green's functions (Cohee and Beroza, 1994). The fourth and fifth panels show the two best-fitting solutions of the three-window approach, which differ only in the rupture velocity used to establish the timing of the first window. In both solutions, the multi-window approach recovers the variable rise time and rupture velocity by distributing slip across the three windows. The slip amplitude solution locates the slip correctly for the long rise-time (4 s) asperities, but tends to mislocate the slip in the shorter rise-time patches. In general, the corresponding rupture time model is a more accurate representation of the input model than a constant propagation velocity, but some artifacts are introduced to reconcile the mislocated slip (for example, between 5 and 15 km).

One practical problem encountered with the three time-window approach is that the fit to seismograms is nearly constant over a wide range of rupture velocity (we refer here to the timing of the first window, not the centroid of the three windows). This is expected because slip is simply shifted to later time-windows when using a higher rupture velocity. However, even though the slip distributions are quite similar for the two cases shown, the rupture time models demonstrate important differences. These differences using noise-free data demonstrate a best-case scenario with this method. Thus without additional information, it is unlikely that fine details of the rupture propagation can be recovered.

We quantify the fit to the data using a weighted measure of variance reduction ($\Delta\sigma^2$) between the model and data defined as

$$\Delta\sigma^2 = \left(1 - \frac{(\boldsymbol{d} - \boldsymbol{g}(\boldsymbol{m}))^T \boldsymbol{C}_d^{-1} (\boldsymbol{d} - \boldsymbol{g}(\boldsymbol{m}))}{\boldsymbol{d}^T \boldsymbol{C}_d^{-1} \boldsymbol{d}}\right) \times 100\%$$

where $\boldsymbol{C}_d^{-1}$ represents the weighting (inverse data covariance) matrix, $\boldsymbol{d}$ is the data vector, and $\boldsymbol{g}(\boldsymbol{m})$ is the model prediction for model $\boldsymbol{m}$. In the noise-free test case the fit to seismograms is better using the three time-window inversion ($\Delta\sigma^2$ = 92% at 2.8 km/s), compared with that obtained with the single-window inversion ($\Delta\sigma^2$ = 73% at 2.4 km/s). In all preferred solutions, the seismic moment is overestimated by 10 to 20%.

To carry out a more realistic test, we add Gaussian white noise to the synthetic data. The power spectra of the noise is flat and is filtered the same as the data. The amplitude of noise is adjusted to reproduce the level of variance reduction (approximately 30%) found when modeling the Landers mainshock data and the Landers aftershocks (Cohee and Beroza, 1994). Note that the level of variance reduction is

strongly dependent on the passband and is considerably higher at lower frequencies. Synthetic displacement seismograms computed using the model shown in fig. 3 (top) are plotted in fig. 4 for three representative strong-motion stations. The solid seismograms are the noise-free synthetic data, and the dashed seismograms are with noise added. The noise is uncorrelated for each component and each station and is not associated with the arrival of any particular phase, so the variance reduction achieved using this synthetic data is a conservative estimate of the modeled signal relative to the actual Landers data. In other words, the true data have relatively greater misfit in that portion of the seismogram containing signal.

The inversion results using the noisy data are shown in fig. 5. Again the one time-window approach recovers the average rupture velocity (2.3 to 2.4 km/s). Recovery of the input slip distribution is degraded slightly relative to the noise-free solution for those asperities with a long (4 s) rise time. The moment is again overestimated by 20%. However, even in the presence of noise, the patches with 2 and 3 s rise times are accurately located. With noise added, the seismogram variance reduction is reduced from 73% to 28%. In contrast, the results using the three-window method have changed considerably from the noise-free case. The slip is located less accurately for all slip patches. In particular, the long rise time

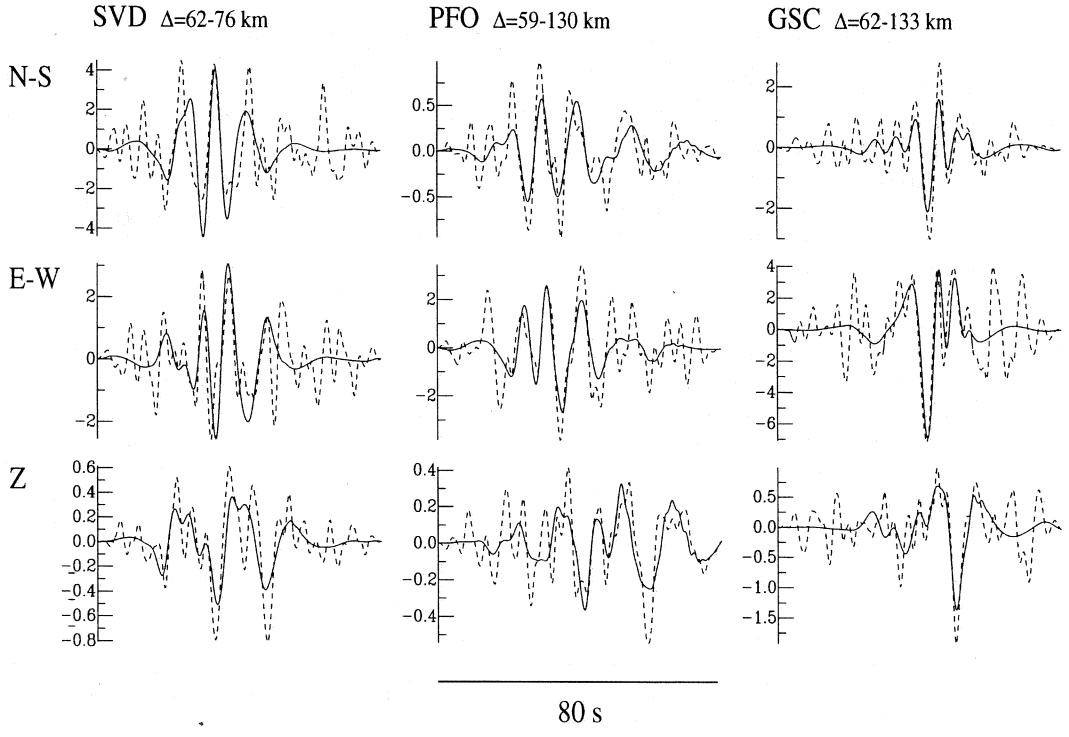

Fig. 4. Synthetic displacement seismograms from the hypothetical Landers earthquake shown in fig. 3 (top) for three seismic stations at representative azimuths (see fig. 2). The synthetic data is shown with and without noise added. In each case, the seismograms are filtered the same as the recorded data (see text). The level of noise was chosen to be representative of the uncorrelated noise present in the Landers mainshock seismograms.

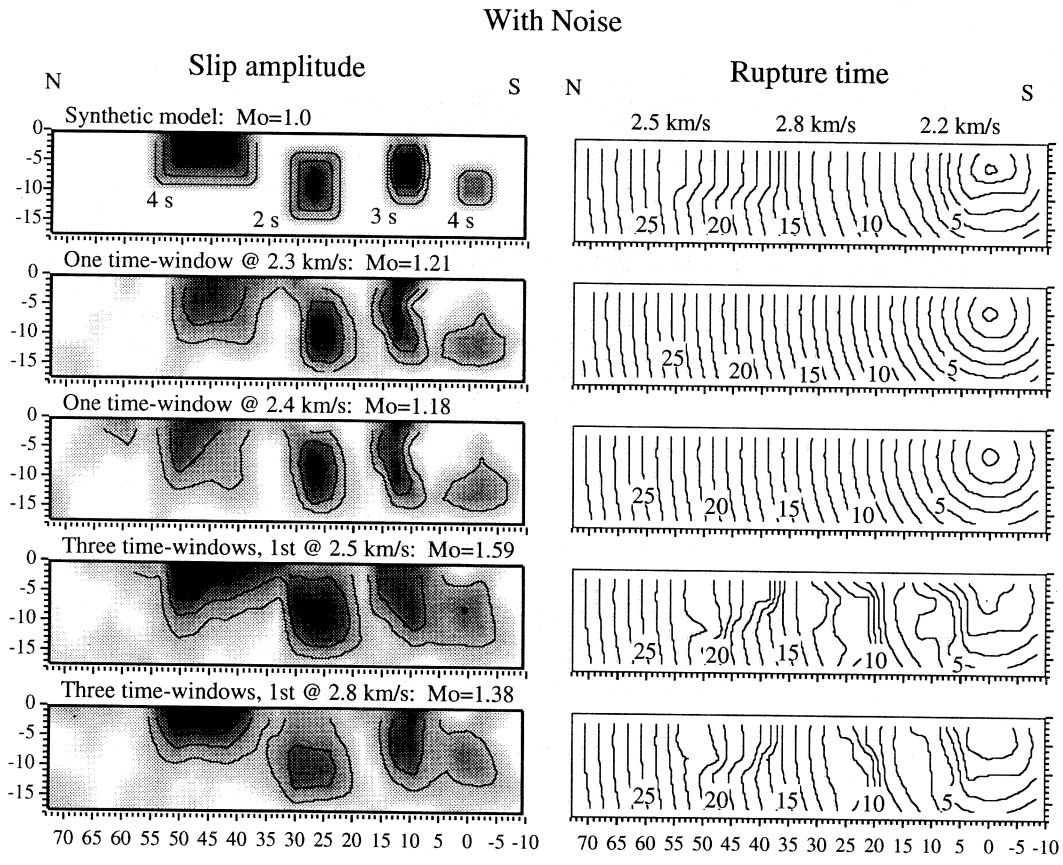

Fig. 5. This figure is analogous to fig. 3, but the inversion results are obtained using synthetic data with noise added. The top panel is the input synthetic test model (slip amplitude-left and rupture time-right). The second and third panels are the results using the single-window method and rupture velocities of 2.3 and 2.4 km/s. The fourth and fifth panels are three time-window solutions using rupture velocities of 2.5 and 2.8 km/s.

patches now have considerable slip in neighboring elements and the asperity is poorly imaged. Compared with the one-window solutions, there is substantially more slip (and seismic moment) in these models, indicating that the increased number of free parameters allows the inversion to fit the uncorrelated noise with erroneous slip. As a result, the total seismic moment is overestimated by about 50%. This overestimation of seismic moment was also found by Hartzell (1989) using a multi-window approach. As noted earlier, he found the seismic moment increased with the addition of each successive time window. Most importantly however, the rupture time solution now bears little resemblance to the input model. The measure of fit to the seismograms is only marginally improved over the one-window model (32% versus 28%).

The estimated seismic moment and fit to seismograms for the synthetic tests are summarized in fig. 6. The top panel shows the moment obtained for a range of rupture velocities (1.8 to 3.5 km/s) using the one time-window

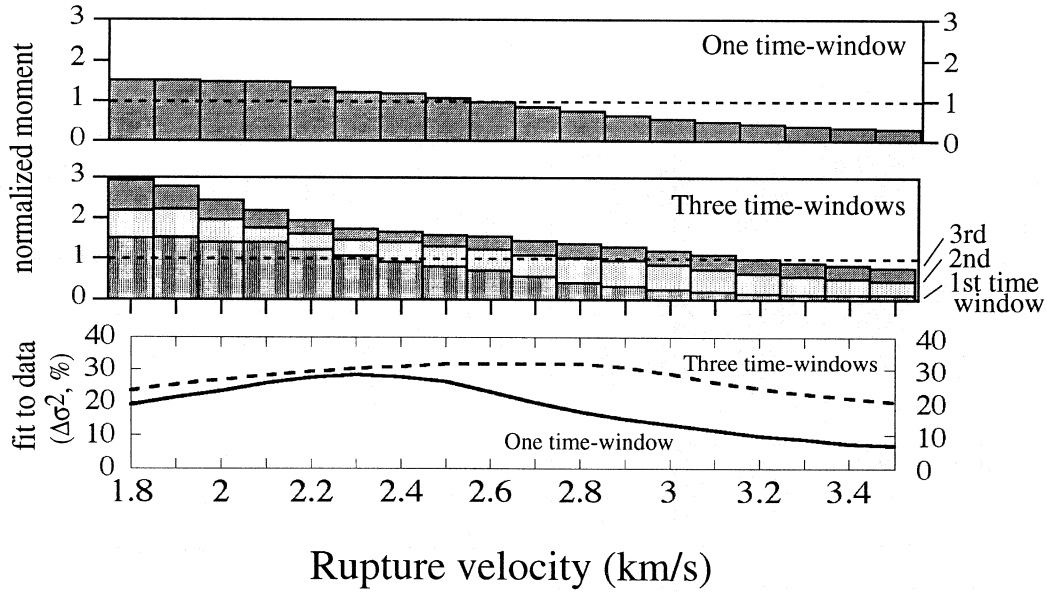

Fig. 6. The seismic moment obtained for each average rupture velocity is shown in the top bar chart for the one time-window model (the input moment is normalized to unity). The moment in each time-window is shown for the three-window model in the middle bar chart. The bottom panel shows the seismogram variance reduction ($\Delta\sigma^2$) as a function of rupture velocity using each method.

inversion. The middle panel shows the moment in each time window using the three-window approach. Note that as the rupture velocity is increased (in the range from 2.4 to 3.0 km/s), the method places a greater percentage of moment in the second and third windows. The bottom panel quantifies the fit to the synthetic data using both inversion methods (solid – one window, dashed – three windows). The broad peak in the variance reduction using the three-window method makes it difficult to choose a best average rupture velocity and is indicative of the increased non-uniqueness that is inherent in the multi-window approach. In contrast, the single-window method has a peak in variance reduction at 2.3 to 2.4 km/s and a corresponding seismic moment that is within 20% of the true moment. The fit to the synthetic data is plotted in fig. 7 for the one-window (2.4 km/s) and three-window (first window at 2.5 km/s) solutions presented in fig. 5. Differences in the visual fit to the data are quite subtle, however close examination reveals the three-window model fits more of the noise in the seismograms.

Finally, we evaluate the ability of the linearized inversion to recover the rupture time model using three different assumed slip distributions. The top panel in fig. 8 is again the synthetic (input) rupture time model. The next panel is the solution of the linearized inversion assuming the true slip distribution and noise-free data. Most features of the input model are recovered, including the delayed rupture in the fourth slip patch at 45 km along strike, and the different rupture velocity on each fault segment. When the noise is added to the data, the solution is worse (third panel), but still contains the principal features of the input model. In practice, we do not know the true slip distribution, and instead use the estimate from the linear one-window inversion at a rupture velocity of 2.4 km/s. This result is shown using both noise-free and noisy synthetic data assum-

ing the two slip models shown in figs. 3 and 5. Both of these inversions recover the true rupture variation to some extent, however the fit to the seismograms is only slightly improved. This suggests that some of the variations in rupture time were mapped as mislocated slip in the previous linear inversion. Note that when we know the correct slip distribution, we recover the input rupture time variation, suggesting that if we can determine the slip distribution using independent methods (*e.g.* geodetic), we can more reliably image the details of the rupture propagation. Elsewhere, we adopted this approach in modeling seismograms of the Landers earthquake by employing geodetic measurements and the mapped surface offsets to establish the distribution of coseismic displacement on the fault (Cohee *et al.*, 1993).

In summary then, the tests with synthetic data have revealed important features attributable to each model parameterization and inversion method: 1) the single-window method tends to overestimate the seismic moment by about 20%, while the multi-window method overestimates the moment by up to 60%; 2) the multi-window parameterization of

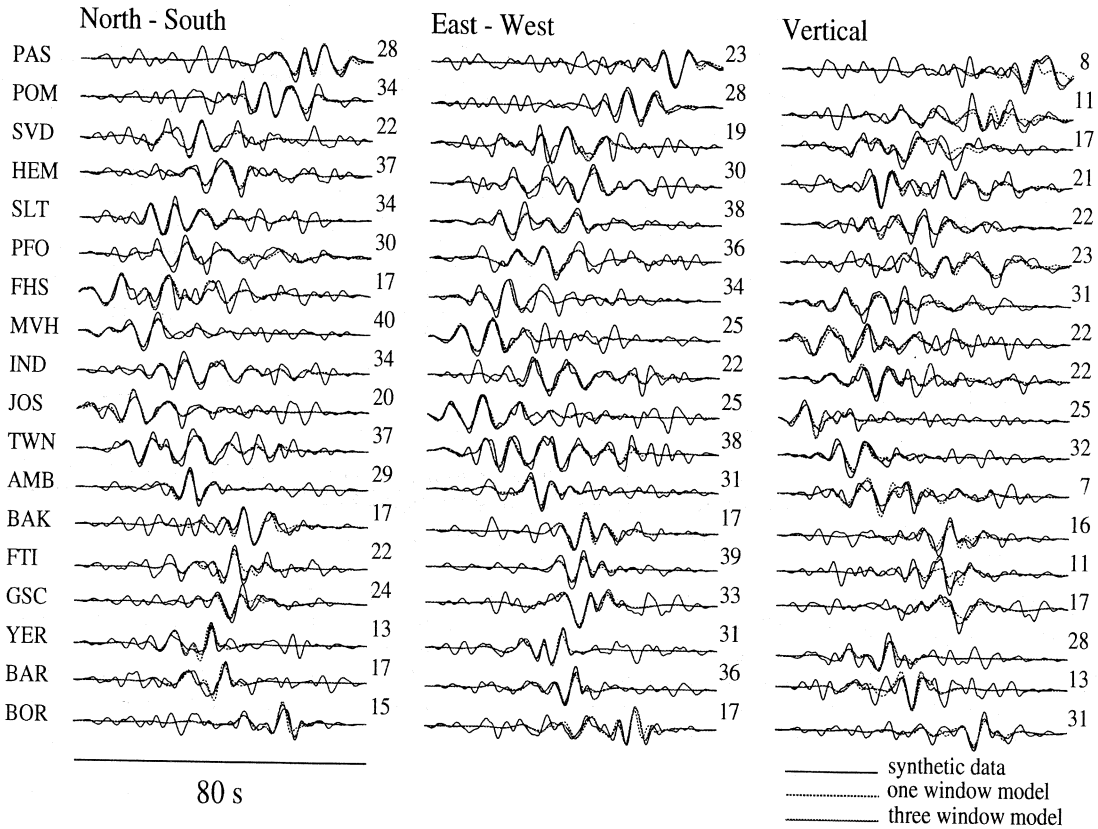

Fig. 7. Fit to synthetic data seismograms for two inversion solutions shown in fig. 5. The solid seismograms are the synthetic data, the dashed seismograms are from the one time-window model (v = 2.4 km/s), and the gray seismograms are from the three time-window model (first window at 2.5 km/s). The variance reduction ($\Delta\sigma^2$) for each station component is listed to the right of the corresponding seismograms for the one-window solution. The average weighted variance reduction is 27.6% using one window, and 31.8% using three windows.

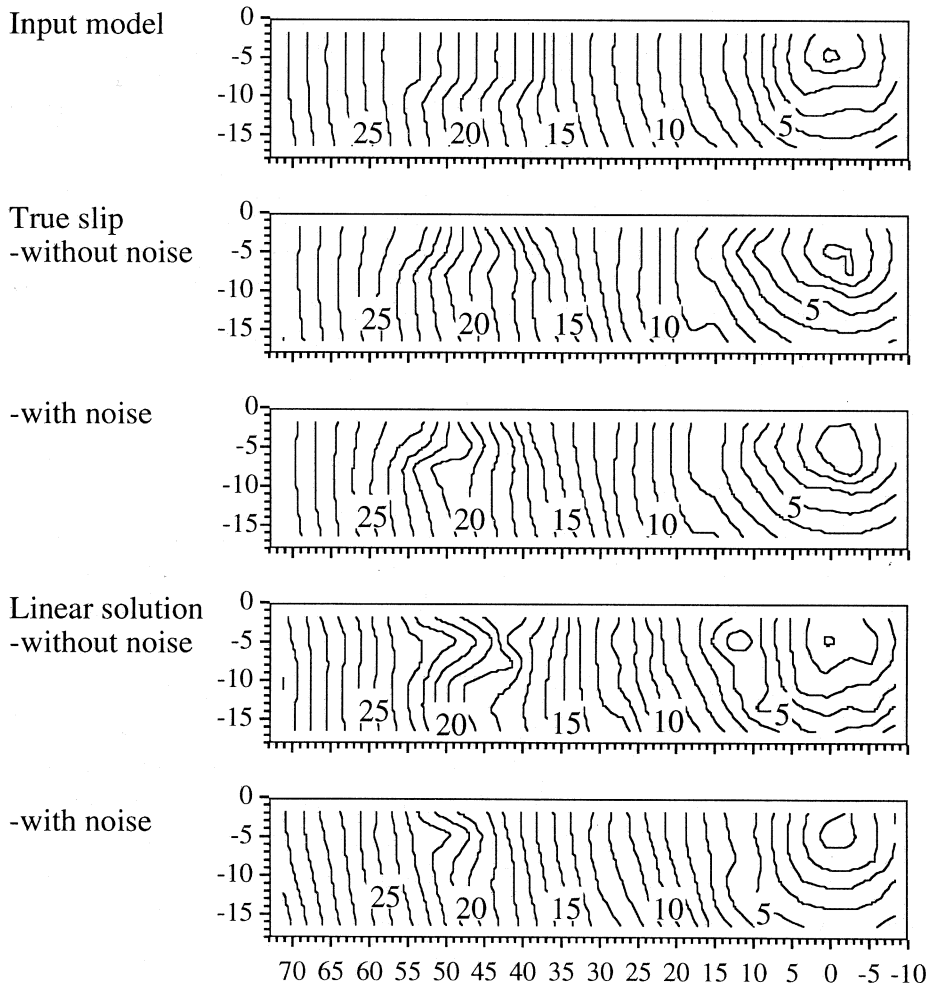

Fig. 8. Four results of the nonlinear inversion for rupture time. The results differ only in the slip distribution assumed in each case, and whether or not noise was added to the synthetic data. The top panel shows the input rupture time model, which is the same as that shown in figs. 3 and 5 (top right). The second and third panels assume the true slip model is known, and use a starting rupture model with a constant rupture velocity. The fourth and fifth panels also use a starting rupture model with a constant rupture velocity, but assume the slip distribution model determined in the corresponding linear single-window inversion.

rupture propagation works well with noise-free data, but produces erroneous results when the data contains noise; 3) the single-window approach is a simpler parameterization of the rupture propagation and consequently can only recover average rupture time characteristics; 4) the slip distribution is, in general, well-recovered using either method; 5) without noise in the data, the single-window approach does better at accurately locating the slip when rise time is more uniform, and the multi-window approach does better when rise time is strongly

variable; 6) with noise in the data, the single window approach more accurately locates the distribution of slip amplitude; and 7) the non-linear inversion for rupture time works well only if the assumed slip distribution is a good approximation of the true slip distribution. Having performed these sensitivity tests using the Landers fault geometry, station distribution, and data passband, we are now in a much better position to carry out the same inversions on the real Landers earthquake data and to interpret the results.

5. Application to the 1992 Landers earthquake

5.1. *Slip amplitude distribution*

Using the recorded strong-motion data of the Landers earthquake, we perform the linear inversion for fault slip using a range of average rupture velocities, v, and evaluate each solution by its fit to the seismic data and the mapped surface slip of Ponti (1992). Solutions from the single-window method are shown in fig. 9a. We see that the location of slip is strongly dependent on rupture velocity so that the surface slip provides a useful constraint on the true v. Although there are near-surface effects that can cause the surface measurements to differ from the average slip in the adjacent 3×3 km^2 cross-section of the fault, we expect that the most representative v is that which yields the highest correlation with the mapped surface slip.

The bottom panel in fig. 9b shows that the fit to seismograms is peaked in the range from 2.4 to 2.7 km/s, with an average rupture velocity of 2.5 km/s providing the best fit. In this example, the surface slip is not explicitly used in the inverse problem, but it provides a useful independent check on the solution. A 2.5 km/s rupture velocity shows good agreement with the mapped surface displacement, although a slightly higher value (2.6 km/s) attains the best correlation. Because the quantitative comparison of predicted to observed surface slip is only sampled every 3 km, the fit is spatially aliased and this small difference is insignificant. Also shown in fig. 9b is the seismic moment obtained using the different values of v. The moment is fairly constant (5 to 7×10^{19} N – m) for v less than 2.9 km/s.

Figure 10a,b is analogous to fig. 9a,b except the multi-window approach is used. With three windows, the trade-off between slip amplitude and v is less pronounced because the method distributes displacement across the time windows. For example, the slip distributions using v = 2.6 and 2.9 km/s in fig. 10a are very similar. But when v = 2.6 km/s most slip occurs in the first window, and when v = 2.9 km/s the slip occurs equally in the first and second windows. This is shown in fig. 10b where the moment in each time window is plotted for each rupture velocity tested. As seen before in the tests with synthetic data, the greater modeling flexibility of the multi-window method is evident in the relative uniformity of variance reduction for a wide range of rupture velocity. This is in contrast to fig. 9b where there is a clear maximum in the seismogram variance reduction at 2.5 km/s. The fit to the surface slip using the three time-window method does not help constrain the rupture velocity. This occurs primarily because for all values of v the predicted surface displacements are larger than the observed, so the largest surface slip variance reduction occurs when the moment is smallest (at v = 3.5 km/s).

A comparison of figs. 9a,b and 10a,b also reveals two other familiar characteristics of the slip distribution and seismogram variance reduction that were found in the solutions with synthetic data. The seismic moment is larger, but the seismogram fit is only slightly improved using three time-windows. Recall that in the sensitivity test, the moment obtained using one time-window was 20% larger than the true moment, while the three time-window model overestimated the input moment by 40 to 60%.

The optimal models using each inversion method are shown in fig. 11a-d. The best-fitting, single time-window solution (v = 2.5 km/s) is shown in fig. 11a. The largest displacement is 38 km north of the hypocenter and begins approximately 16 s after the initiation of rupture. This model includes the surface slip

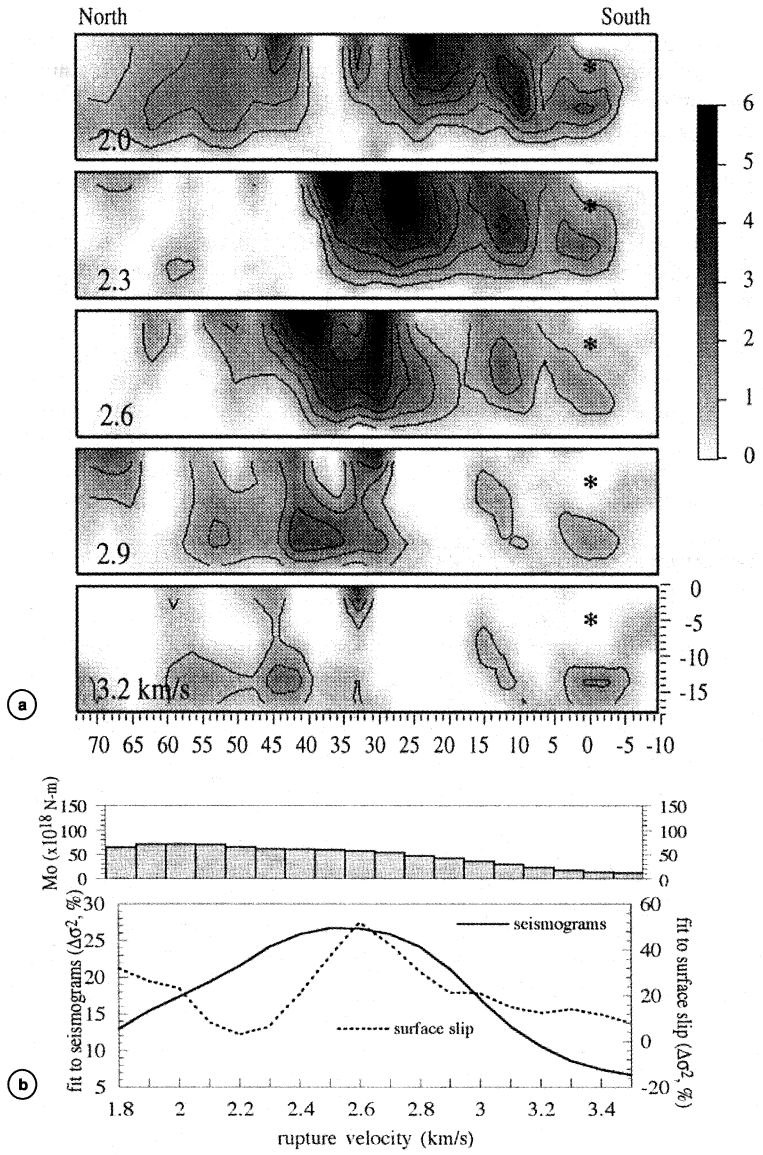

Fig. 9a,b. Comparison of fault slip solutions for the 1992 Landers earthquake using the single-window method and different average rupture velocities, and the corresponding agreement with the mapped surface slip. A rupture velocity of 2.5 km/s gives the best fit to the seismograms and an acceptable fit to the surface slip. a) Right-lateral slip amplitude solutions obtained for rupture velocities of 2.0, 2.3, 2.6, 2.9, and 3.2 km/s. The grayscale bar to the right and the 1 m contours indicate right-lateral displacement on the fault surface. Slip is summed for the overlapping portions of the fault. The hypocenter defines the horizontal origin and is indicated by a symbol at 4.5 km depth. b) Variance reduction ($\Delta\sigma^2$) as a function of rupture velocity for both the fit to seismograms and the fit to surface slip. The seismic moment obtained for each rupture velocity is shown in the bar chart with units of 10^{18} N-m.

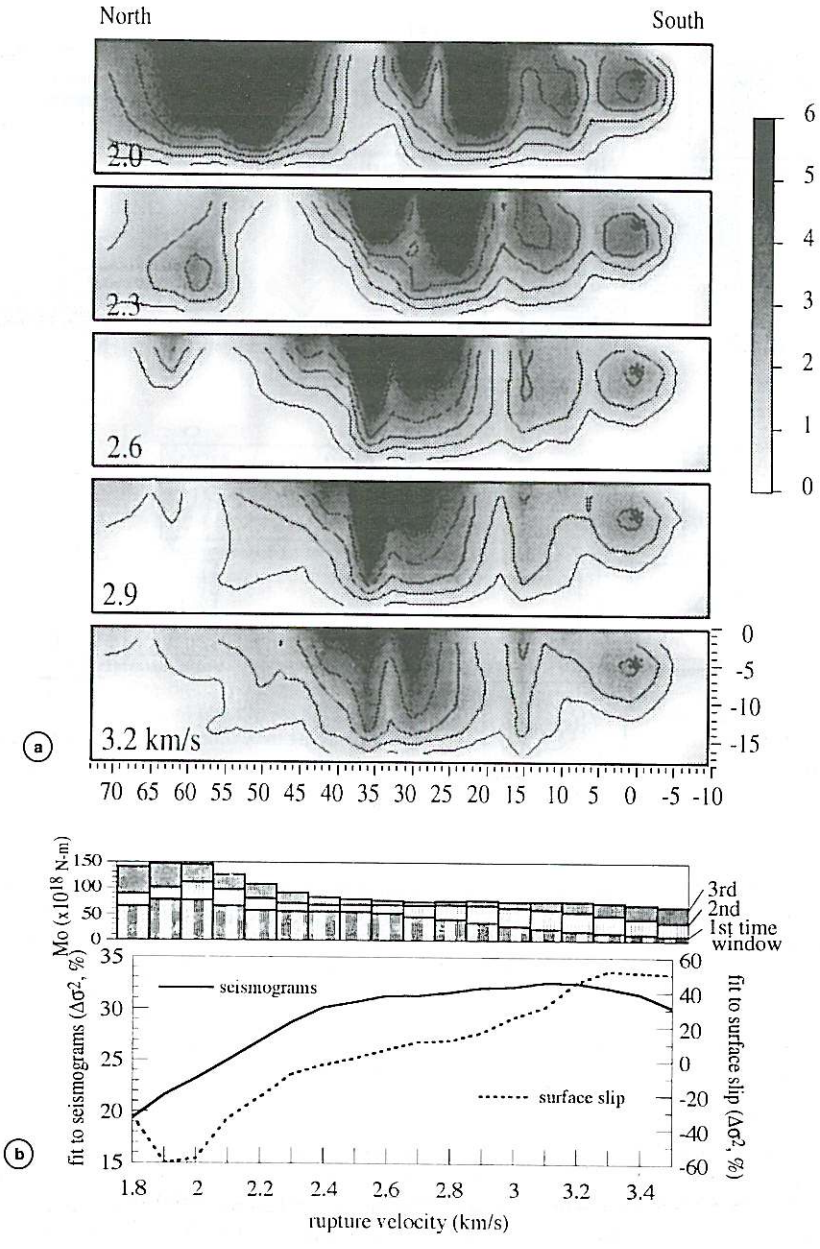

Fig. 10a,b. This figure is analogous to fig. 9a, b, but using the three-window inversion method. a) Slip amplitude solutions obtained for average rupture velocities of 2.0, 2.3, 2.6, 2.9, and 3.2 km/s. The grayscale bar to the right and the 1 m contours indicate right-lateral displacement on the fault surface. b) Variance reduction ($\Delta\sigma^2$) as a function of rupture velocity for both the fit to seismograms and the fit to surface slip. The seismic moment obtained in each of the three time-windows is shown in the bar chart. The moment is nearly constant (7 to 8 $\times$ 10^{19} N-m) for rupture velocities greater than 2.3 km/s.

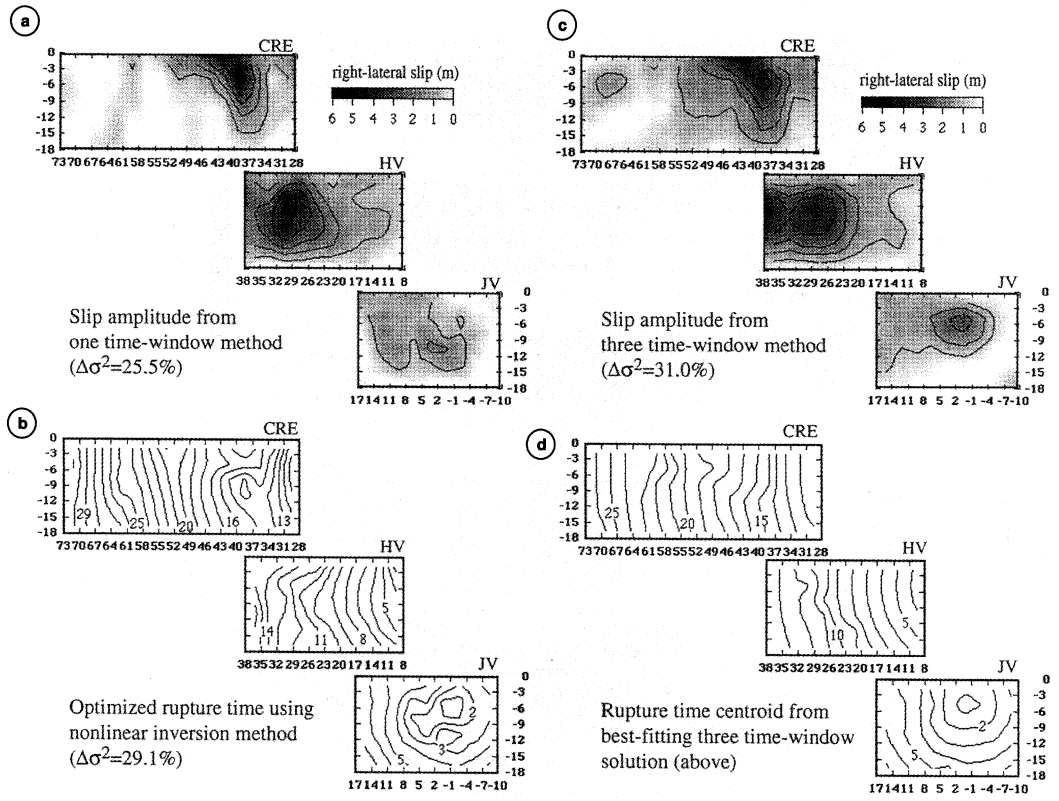

Fig. 11a-d. Best-fitting slip amplitude and rupture time models for the Landers earthquake. The three fault segments from north to south are representative of the Camp Rock-Emerson (CRE), the Homestead Valley (HV), and the Johnson Valley (JV) faults. a) Three fault segment cross-section of right-lateral slip amplitude obtained with the one time-window method and a rupture velocity of 2.5 km/s. The grayscale bar and the 1 m slip contours show displacement on the fault surface. The seismic moment is 6×10^{19} N-m. b) Contours of rupture time obtained using the linearized inversion assuming the above slip model. Contour interval is 1 s. c) Cross-section of best-fitting slip model obtained using the three time-window method and a first-window rupture velocity of 2.8 km/s. The moment of this model is 8×10^{19} N-m. d) Contours of the rupture time centroid from the solution in fig. 11c (for elements with slip greater than 1.5 m).

boundary condition. Adding this boundary condition yields a very similar solution at depths greater than 3 km, but also conforms to the mapped slip at the ground surface. The decrease in variance reduction from adding this constraint is quite small (1.2%).

The best-fitting, three time-window slip distribution model (v = 2.8 km/s) is shown in fig. 11c. This slip model is very similar to fig. 11a on the Camp Rock-Emerson and Homestead Valley fault segments north of the hypocenter. The greatest differences exist on the Johnson Valley segment where the three-window solution has more than 3 m of displacement at the hypocenter. In comparison, the single window model has less than 1 m of slip amplitude near the hypocenter.

The total seismic moment for the single-window model is 6×10^{19} N-m, for the three-window model it is 8×10^{19} N-m. Moments determined in other studies range from 7 to 11×10^{19} N-m. See Cohee and Beroza (1994)

for a summary. Although the moment obtained with three time-windows is in better agreement with the other estimates, our results from the sensitivity tests suggests this method tends to overestimate the actual moment required by the strong-motion data. The better agreement between the moment of the multi-window model and the moment derived from studies of other data sets is likely to be strongly influenced by the regularization used. This relative insensitivity to moment is demonstrated by the fact that the multi-window model has a considerably larger moment than the single-window model, yet the fit to the seismograms is nearly identical.

The fit to the Landers seismograms is shown in fig. 12 from the one-window ($\Delta\sigma^2$ = 25.5%) and three-window ($\Delta\sigma^2$ = 31.0%) solutions shown in fig. 11a-d. The data are shown as solid lines and the model seismograms are dashed (one window) and gray (three windows). Both data and model seismograms are plotted at the same scale and the amplitude is normalized to the largest seismogram peak. The variance reduction is listed at the right of each seismogram for the single-window result. Because each sta-

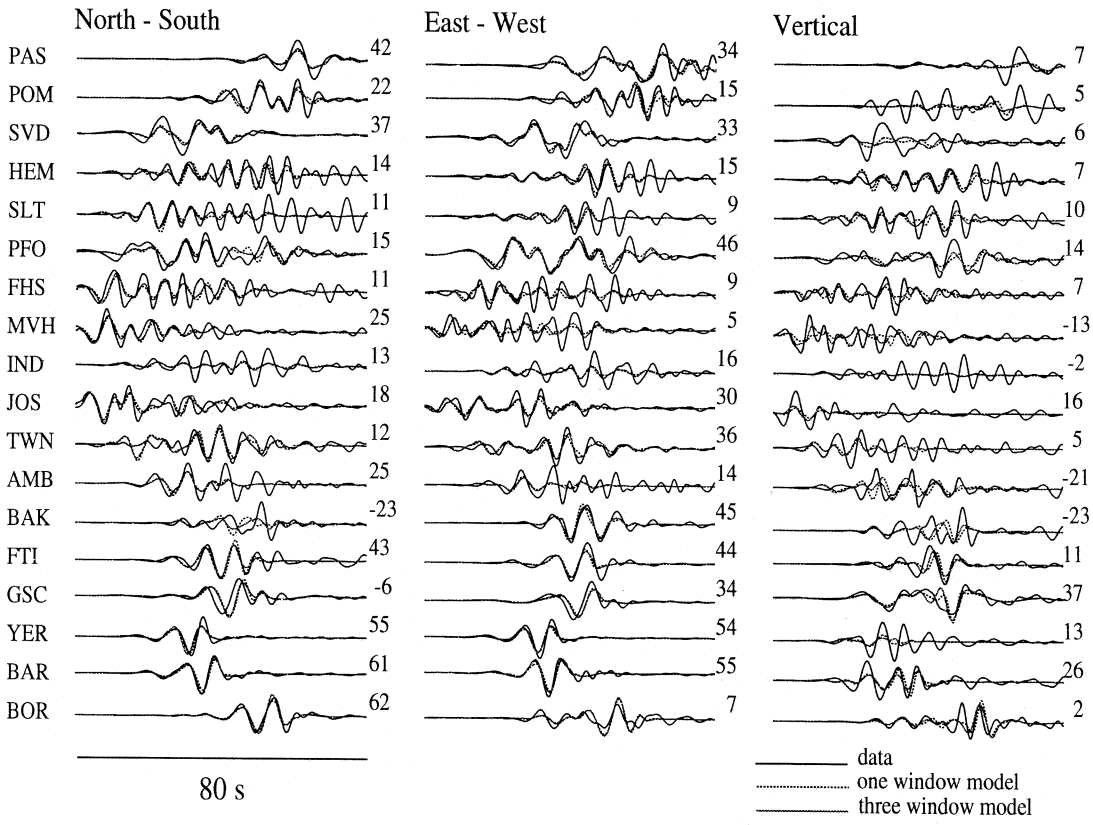

Fig. 12. Fit to the recorded displacement seismograms using the linear solutions shown in figs. 11a and 11c-d. The data seismograms (solid) and model seismograms (one window-dashed, three windows-gray) are plotted at the same amplitude scale. The variance reduction ($\Delta\sigma^2$) for each station component is listed to the right of the corresponding seismograms for the one-window solution. The average weighted variance reduction is 25.5% using one window and 31.0% using three windows.

tion holds equal weight and each component is weighted proportional to its power, the largest amplitude horizontal components show the largest variance reduction. Most of the seismograms are fit well, including the peak amplitudes, which vary from 0.7 to 28.1 cm (see fig. 2).

5.2. *Rupture propagation*

We use the linear solution obtained with a constant rupture velocity of 2.5 km/s (fig. 11a) as the initial model in a linearized inversion to optimize the rupture time of each fault element. Recall that with the single-window approach, we separate the inversion for slip amplitude and rupture time to avoid the problem of relative weighting. However, because we first solve for slip and then for rupture time, the procedure favors a variable slip model, with the spatial roughness determined by the smoothing weight. The result of the linearized inversion for rupture time is shown in fig. 11b. The model shown in fig. 11b produced the largest increase in variance reduction for the smallest rupture time perturbations.

Allowing these small perturbations (< 2 s) to the average rupture velocity starting model increases the variance reduction modestly from 25.5 to 29.1%. The data and model covariance are not known, but we do know that measurement error is small compared with theoretical error introduced by inaccurate Green's functions, and we also know that we are near the limit of how well we expect to fit the data based on the modeling of aftershock waveforms in Cohee and Beroza (1994).

The rupture time model from the three-window inversion is shown in fig. 11d. The slip model has the same smoothing and boundary conditions as the single-window solution (fig. 11a). The timing of the first window is fixed using a rupture velocity of 2.8 km/s, which produced the greatest variance reduction. We define the rupture time in the multi-window model to be the slip-weighted temporal centroid for elements with slip greater than 1.5 m. In fig. 11d we contour this centroid for comparison with fig. 11b.

Based on the sensitivity tests, it is difficult to give strong preference to either rupture time model. It is very likely that the single-window method recovers a reliable average rupture velocity of 2.5 km/s. Our results with synthetic data suggest that details of these rupture propagation images are not particularly reliable due to the strong trade-off between slip amplitude and rupture time. Recovering the time-dependent behavior of the rupture is difficult for the Landers earthquake because the large source-receiver distances require using long-period (≥ 4 s) waveforms dominated by regional surface waves rather then body waves. One other lesson from the tests with synthetic data is that we can recover rupture time details if we can obtain the slip distribution correctly using other constraints (*e.g.* geodetic).

There are some general features that are common to both rupture models in fig. 11a-d. Rupture of the Johnson Valley segment in the hypocentral region is relatively fast. Fast rupture of this segment could be facilitated by the dynamic stresses generated by the immediate foreshock that brought the fault closer to failure as the mainshock rupture began to propagate northward. The rupture across the southern part of the Homestead Valley segment is similar to the constant rupture velocity model. At the high-slip region on the north end of this segment, the rupture velocity decreases somewhat, then increases as it propagates across the region of highest slip. In both models, rupture on the Camp Rock-Emerson segment initiates 1-2 s earlier than the constant velocity model. On the Camp Rock-Emerson segment the rupture front propagates at higher velocity at depth than near the surface and ruptures through the shallow, high-slip region from below. The observation that the rupture front slows down as it encounters high-slip regions suggests that they were relatively further from failure before the mainshock either due to lower pre-stress, higher strength, or both (Beroza and Spudich, 1988).

6. Summary

In this study we compared two different approaches for recovering the rupture behavior of

a fault using strong-motion seismograms. We first analyzed the properties of the solutions and their ability to recover a general rupture model in the presence of a realistic level of noise. The results of the synthetic tests indicate both methods have strengths and weaknesses.

One strength of the single-window method is that it appears to recover the seismic moment fairly well. It also recovers the average rupture velocity and variations in slip amplitude provided the rise time is short relative to the periods used in the analysis. The weaknesses of the single-window approach are that it does not recover the slip properly when the rise time is long, and that it does not recover detailed variations in rupture velocity.

One strength of the multi-window case is that it has the flexibility to correctly locate displacement in the presence of substantial rise time variability. The weaknesses of this method are that it tends to overestimate the seismic moment and that, like the single-window method, it does not reliably recover details of the rupture propagation.

Despite these caveats, there is much similarity in the slip amplitude solutions for the Landers earthquake. Using both methods, the slip distribution is heterogeneous, with high slip regions in the same general region of each fault segment. The three-window result has a 20% larger seismic moment than the one-window result. This difference is similar to that found in the sensitivity test, and reflects the tendency of the multi-window approach to overestimate the actual moment required by the strong-motion data. Although recovery of detailed variations in rupture velocity were problematic in the sensitivity tests, the two models derived from the Landers data do show some similarities in the propagation of rupture. Both models suggest high velocities near the hypocenter, nearly constant rupture velocity on the Homestead Valley fault segment, and some delay in rupture propagation on the southern Camp Rock-Emerson segment.

It is clear from the comparison of the one- and three-window models for both the synthetic test case and for the Landers earthquake data, that strong-motion seismograms alone cannot estimate the seismic moment with great precision. In both cases the fit to the data was nearly identical, yet the seismic moment differed by up to 50%. In short, we find that strong-motion data are not particularly sensitive to the seismic moment (compared to other data), and that moments obtained using strong-motion seismograms are strongly influenced by the choice of model parameterization and inversion method.

Cohee *et al.* (1993) assumed a geodetically derived slip distribution and used strong-motion seismograms to recover characteristics of the rupture propagation in a linearized inversion. Although we did not assess the uncertainty of the geodetically derived slip model, it was evident that including geodetic data helped reduce the trade-off between slip amplitude and rupture time that affect solutions based on seismic data alone. Clearly, including other types of data will increase the solution accuracy and decrease non-uniqueness in future studies.

Acknowledgements

We thank the California Strong Motion Instrumentation Program, TERRAscope, S. Hough of the U.S. Geological Survey, and Southern California Edison for releasing seismograms soon after the earthquake. We appreciate comments on the manuscript from an anonymous reviewer, and acknowledge partial funding from a NSF Presidential Young Investigator award (GCB).

REFERENCES

Abercrombie, R. and J. Mori (1994): Local observations of the onset of a large earthquake: 28 June 1992 Landers, California, *Bull. Seismol. Soc. Am.*, **84**, 725-734.

Beroza, G.C. (1991): Near-source modeling of the Loma Prieta earthquake: evidence for heterogeneous slip and implications for earthquake hazard, *Bull. Seismol. Soc. Am.*, **81**, 1603-1621.

Beroza, G.C. and P. Spudich (1988): Linearized inversion for fault rupture behavior: application to the 1984 Morgan Hill, California, earthquake, *J. Geophys. Res.*, **93**, 6275-6296.

Cohee, B.P., J. Freymueller, G.C. Beroza and P. Segall (1993): Complementary inversion for earthquake rupture using near-source seismic and geodetic observations: application to 1992 Landers earthquake, *EOS Trans. Am. Geophys. Union*, **74**, 429.

COHEE, B.P. and G.C. BEROZA (1994): Slip distribution of the 1992 Landers earthquake and its implications for earthquake source mechanics, *Bull. Seismol. Soc. Am.*, **84**, 692-712.

COCCO, M. and F. PACOR (1993): The rupture process of the 1980 Irpinia, Italy, earthquake from the inversion of strong motion waveforms, *Tectonophysics*, **218**, 157-177.

CSMIP (1992): Processed CSMIP strong-motion records from the Landers, California earthquake of June 28, 1992; OSMS 92-09, 92-11, 92-13, 93-01, *Calif. Dept. of Conserv. Reports*, Sacramento, CA.

DAY, S.M. (1982): Three-dimensional finite-difference simulation of fault dynamics: rectangular faults with fixed rupture velocity, *Bull. Seismol. Soc. Am.*, **72**, 705-727.

DREGER, D.S. (1994): Investigation of the rupture process of the 28 June 1992 Landers earthquake utilizing TERRAscope, *Bull. Seismol. Soc. Am.*, **84**, 713-724.

FRANKEL, A. (1992): Comment on «Rupture process of the 1987 Superstition Hills earthquake from the inversion of strong-motion data» by D.J. WALD, D. V. HELMBERGER and S.H. HARTZELL, *Bull. Seismol. Soc. Am.*, **82**, 1511-1518.

FRANKEL, A. and L. WENNERBERG (1989): Rupture process of the M_s 6.6 Superstition Hills, California, earthquake determined from strong-motion recordings: application of tomographic source inversion, *Bull. Seismol. Soc. Am.*, **79**, 515-541.

FUKUYAMA, E. and K. IRIKURA (1986): Rupture process of the 1983 Japan Sea (Akita-Oki) earthquake using a waveform inversion method, *Bull. Seismol. Soc. Am.*, **76**, 1623-1640.

HARTZELL, S. (1989): Comparison of seismic waveform inversion results for the rupture history of a finite fault: application to the 1986 North Palm Springs, California, earthquake, *J. Geophys. Res.*, **94**, 7515-7534.

HARTZELL, S.H. and T.H. HEATON (1983): Inversion of strong ground motion and teleseismic waveform data for the fault rupture history of the 1979 Imperial Valley, California, earthquake, *Bull. Seismol. Soc. Am.*, **73**, 1553-1583.

HARTZELL, S. and T. HEATON (1986): Rupture history of the 1984 Morgan Hill, California, earthquake from the inversion of strong motion records, *Bull. Seismol. Soc. Am.*, **76**, 649-674.

HARTZELL, S. and M. IDA (1990): Source complexity of the 1987 Whittier Narrows, California, earthquake from the inversion of strong motion records, *J. Geophys. Res.*, **95**, 12475-12485.

HAUKSSON, E., L.M. JONES, K. HUTTON and D. EBERHART-PHILLIPS (1993): The 1992 Landers earthquake sequence: seismological observations, *J. Geophys. Res.*, **98**, 19835-19858.

HEATON, T.H. (1990): Evidence for and implications of self-healing slip pulses in earthquake rupture, *Phys. Earth and Planet. Int*, **64**, 1-20.

HOUGH, S.E., J. MORI, E. SEMBERA, G. GLASSMOYER, C. MUELLER and S. LYDEEN (1993): Southern surface rupture associated with the 1992 M7.4 Landers earthquake: did it all happen during the mainshock? *Geophys. Res. Lett.*, **20**, 2615-2618.

JOHNSON, A.M., R.W. FLEMING and K.M. CRUIKSHANK (1994): Shear zones formed along long, straight traces of fault zones during the 28 June 1992 Landers, California, earthquake, *Bull. Seismol. Soc. Am.*, **84**, 499-510.

KANAMORI, H., H.-K. THIO, D. DREGER, E. HAUKSSON and T. HEATON (1992): Initial investigation of the Landers, California earthquake of 28 June 1992 using TERRA scope, *Geophys. Res. Lett.*, **19**, 2267-2270.

LAWSON, C.L. and R.J. HANSON (1974): *Solving Least Squares Problems* (Prentice-Hall, Englewood Cliffs, NJ).

MENDEZ, A.J. and J.E. LUCO (1990): Steady state, near-source models of the Parkfield, Imperial Valley, and Mexicali Valley earthquakes, *J. Geophys. Res.*, **95**, 327-340.

MENDEZ, A.J. and J.G. ANDERSON (1991): The temporal and spatial evolution of the 19 September 1985 Michoacan earthquake as inferred from near-source ground-motion records, *Bull. Seismol. Soc. Am.*, **81**, 844-861.

OLSON, A.H. (1987): A Chebyshev condition for accelerating convergence of iterative tomographic methods – solving large least squares problems, *Phys. Earth Planet. Inter.*, **47**, 333-345.

OLSON, A.H. and R.W. APSEL (1982): Finite faults and inverse theory with applications to the 1979 Imperial Valley earthquake, *Bull. Seismol. Soc. Am.*, **72**, 1969-2001.

PONTI, D.J. (1992): Quaternary chronostratigraphy and deformation history, Los Angeles basin, California, *NEHRP Sum. Tech. Rep.*, **24**, 588-592.

PRESS, W.H., B.P. FLANNERY, S.A. TEUKOLSKY and W.T. VETTERLING (1989): *Numerical Recipes* (Cambridge University Press, Cambridge).

SCHOLZ, C.H. (1990): *The Mechanics of Earthquake Rupture* (Cambridge University Press, Cambridge).

SIEH, K., L. JONES *et al.* (1993): Near-field investigations of the Landers earthquake sequence, April to July 1992, *Science*, **260**, 171-176.

SPAKMAN, W. and G. NOLET (1988): Imaging algorithms, accuracy, and resolution in delay time tomography, in *Mathematical Geophysics* (D. Reidel, Dordrecht), pp. 155-188.

SPUDICH, P.K.P. (1980): The deHoop-Knopoff representation theorem as a linear inverse problem, *Geophys. Res. Letters*, **7**, 717-720.

STEIDL, J.H., R.J. ARCHULETA and S.H. HARTZELL (1991): Rupture history of the 1989 Loma Prieta, California earthquake, *Bull. Seismol. Soc. Am.*, **81**, 1573-1602.

TAKEO, M. (1987): An inversion method to analyze the rupture processes of earthquakes using near-field seismograms, *Bull. Seismol. Soc. Am.*, **77**, 490-513.

WALD, D.J., D. V. HELMBERGER and S.H. HARTZELL (1990): Rupture process of the 1987 Superstition Hills earthquake from the inversion of strong-motion data, *Bull. Seismol. Soc. Am.*, **80**, 1079-1098.

WALD, D.J., D. V. HELMBERGER and T.H. HEATON (1991): Rupture model of the 1989 Loma Prieta earthquake form the inversion of strong-motion and broadband teleseismic data, *Bull. Seismol. Soc. Am.*, **81**, 1540-1572.

WALD, D.J. and T.H. HEATON (1994): Spatial and temporal distribution of slip for the 1992 Landers, California earthquake, *Bull. Seismol. Soc. Am.*, **84**, 668-691.